PROCEEDINGS OF SCIENCE

Measurement of cosmic-ray proton spectrum with the Dark Matter Particle Explorer

Chuan Yue[*1], **Antonio De Benedittis**[2,3], **Mario Nicola Mazziotta**[4], **Stefania Vitillo**[5], **Zhi-Hui Xu**[1,6], **Yu-Hong Yu**[7], **for the DAMPE Collaboration** [†‡]

[1] *Key Laboratory of Dark Matter and Space Astronomy, Purple Mountain Observatory, Chinese Academy of Sciences, Nanjing 210034, China*
[2] *Università del Salento - Dipartimento di Matematica e Fisica "E. De Giorgi", I-73100, Lecce, Italy*
[3] *Istituto Nazionale di Fisica Nucleare (INFN) - Sezione di Lecce, I-73100, Lecce, Italy*
[4] *Istituto Nazionale di Fisica Nucleare (INFN) - Sezione di Bari, I-70125, Bari, Italy*
[5] *Department of Nuclear and Particle Physics, University of Geneva, CH-1211, Switzerland*
[6] *School of Astronomy and Space Science, University of Science and Technology of China, Hefei 230026, China*
[7] *Institute of Modern Physics, Chinese Academy of Sciences, Lanzhou 730000, China*

E-mail: yuechuan@pmo.ac.cn

The precise measurement of the energy spectrum of cosmic ray proton is important for the study of cosmic ray physics. The DArk Matter Particle Explorer (DAMPE), a space-based high energy particle detector, has a very good potential to measure cosmic-ray protons up to 100 TeV. Since its successful launch on December 17, 2015, DAMPE has been operated on-orbit for more than three years. Here, the analysis of the cosmic-ray proton spectrum from 40GeV to 100TeV with DAMPE experiment will be reported.

36th International Cosmic Ray Conference -ICRC2019-
July 24th - August 1st, 2019
Madison, WI, U.S.A.

[*] Speaker.

[†] for collaboration list see PoS(ICRC2019)1177

[‡] The DAMPE mission is funded by the strategic priority science and technology projects in space science of Chinese Academy of Sciences. In China the data analysis was supported in part by the National Key Research and Development Program of China (No. 2016YFA0400200), the National Natural Science Foundation of China (Nos. 11525313, 11622327, 11722328, U1738205, U1738207, U1738208), the strategic priority science and technology projects of Chinese Academy of Sciences (No. XDA15051100), the 100 Talents Program of Chinese Academy of Sciences, and the Young Elite Scientists Sponsorship Program. In Europe the activities and the data analysis are supported by the Swiss National Science Foundation (SNSF), Switzerland; the National Institute for Nuclear Physics (INFN), Italy.

PoS(ICRC2019)163

1. Introduction

Cosmic rays (CRs) with energies up to the so-called "knee" (at $E \sim 3$ PeV [1] where the all-particle spectrum exhibits a spectral softening) are widely believed to be accelerated by strong shocks due to e.g., the supernova explosions. Protons are the most abundant particles in the primary CRs. Precise measurements of the energy spectrum of protons up to PeV energies are essential in understanding the origin and acceleration of them, as well as the physics of the "knee" [2].

Despite at low energy ($E \lesssim 30$ GeV) CRs are significantly affected by the solar modulation, the energy spectrum of CRs above a few tens of GeV according to traditional acceleration and propagation models is expected to follow a featureless power-law. However, Several recent measurements of the proton flux by balloon-borne experiment ATIC-2 [3] and space-borne experiments PAMELA [4], AMS-02 [5] and CALET[6] observed a deviation (hardening) from single power-law distribution at rigidities of ~ 400 GV. These results challenge the conventional picture of the CR production and propagation. Various types of modification of the conventional model have been proposed (e.g., [7, 8]). The precise measurements of the energy spectra of CRs above TeV are thus motivated by the test of potential new spectral features. Interestingly, the recent CREAM and NUCLEON data show hints that the energy spectra of CR nuclei may become softer above rigidities of $10 \sim 20$ TV[9, 10]. Furthermore, the all-particle spectrum measured by the air shower experiment HAWC shows a spectral softening around 40TeV, which should be dominated by the light element, i.e. proton and helium [11].

The DArk Matter Particle Explorer (DAMPE) is a calorimetric-type, satellite-borne detector for high energy electron, γ-ray, and CR observations. The DAMPE detector has a large geometric factor, and is expected to improve significantly the direct measurement of the proton spectrum above TeV [12].

2. DAMPE instrument

The DAMPE detector consists of 4 sub-detectors, which are a Plastic Scintillator strip Detector (PSD), a Silicon-Tungsten tracKer-converter (STK), a BGO imaging calorimeter, and a NeUtron Detector (NUD) from top to bottom [12]. The PSD measures the charge of an incident particle. It can also be used as an anti-coincidence detector for γ-rays. The STK reconstructs the trajectory and measures the charge. The BGO calorimeter measures the energy, and provides electron-hadron identification. The track information can also be obtained via the BGO image. The NUD provides additional electron-hadron discrimination, which is important for energies above TeV. These 4 sub-detectors enable good measurements of the charge ($|Z|$), arrival direction, energy, and particle identity of each event. The major scientific objectives of DAMPE consist of indirect search for dark matter particle, γ-ray astronomy, and studies on origin and propagation of Galactic CRs.

3. Data analysis

Thirty months of DAMPE on-orbit data from January 1^{st}, 2016 to June 30^{th}, 2018 are analyzed in this work. The fraction of live time is about 75.73% after excluding the time when the satellite passes the South Atlantic Anomaly (SAA) region, the instrument dead time, the time for on-orbit

calibration, and the period between September 9, 2017 and September 13, 2017 when a big solar flare occurred and may have affected the baseline of the detector.

3.1 Event Selection

To ensure that all detectors work in good condition, data recorded when the satellite was in the SAA region are excluded. Furthermore, we select events with deposited energy in the calorimeter larger than 20 GeV, to effectively avoid the effect due to the geomagnetic rigidity cutoff [15].

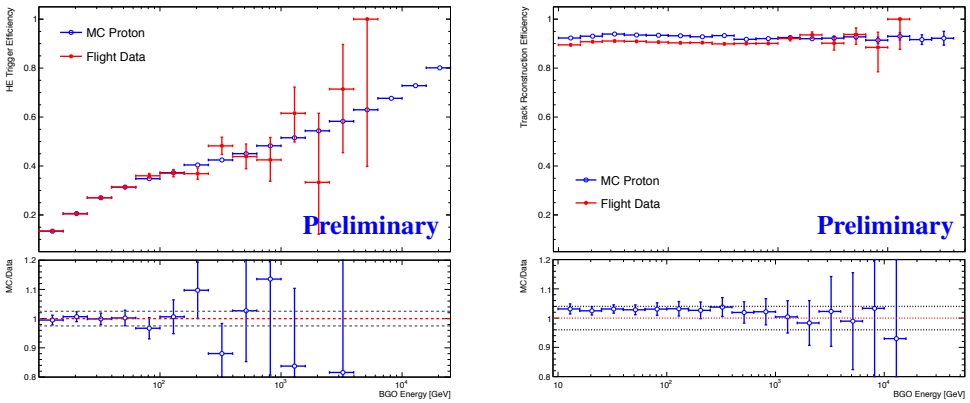

Figure 1: *Left* — The HE trigger efficiency of protons as a function of BGO energy for flight data (red) and MC data (blue). *Right* — The track reconstruction efficiency for flight data (red) and MC data (blue).

- Pre-selection
  The DAMPE has four different triggers implemented on orbit [12]: Unbiased trigger, MIP trigger, High-Energy (HE) trigger and Low-Energy(LE) trigger. The events are required to meet the HE trigger condition in order to make sure the shower development starts at the beginning of the calorimeter. The HE trigger efficiency is estimated by means of unbias trigger sample, which is pre-scaled by 1/512 at low latitudes ($\leqslant \pm 20^{\circ}$) and 1/2048 at high latitudes:
  $$\varepsilon_{\text{trigger}} = \frac{N_{\text{he|unb}}}{N_{\text{unb}}} \tag{3.1}$$
  where N_{unb} is the number of events which pass the proton selection and are triggered as unbiased sample, and $N_{\text{he|unb}}$ is the number of events which pass the HE trigger in the selected unbiased sample N_{unb}. The *left* panel of Figure 1 shows the HE trigger efficiency as a function of deposit energy in the BGO calorimeter (BGO energy). For energies higher than hundreds of GeV, the uncertainty of flight data increases due to the limited statistics of the unbiased sample. The difference between the flight data and the Monte-Carlo (MC) simulation is found to be within $\sim 2.5\%$ below 200 GeV, which is taken as one kind of systematic errors. Apart from the HE trigger, the pre-selection requires at least one hit in each sub-layer of the PSD and one good track in the STK with more than four hits in both X and Y views.

- Track selection
  In case that there are more than one good tracks in the STK, the most reliable one is selected

by jointly considering the following factors: the length of the track, the reduced χ^2 value of the fit, and the match between the candidate track and the shower axis in the calorimeter. The selected track is then required to cross all sub-layers of the PSD and pass through the calorimeter from top to bottom. To estimate the STK track efficiency for proton, a pure proton sample is obtained by applying an independent charge selection based on the reconstructed shower axis in the calorimeter. The *right* panel of Figure 1 shows the track reconstruction efficiency as a function of BGO energy. The results of MC data and flight data are consistent with each other within 3.5% up to 10TeV.

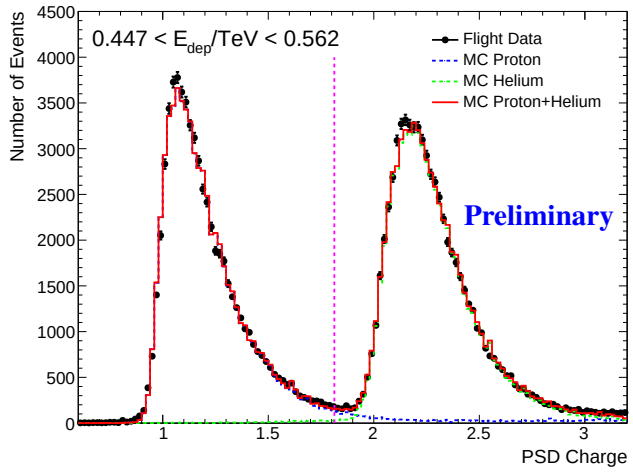

Figure 2: The reconstructed charge distribution for BGO deposited energies of $447-562$ GeV, The on-orbit data (black) are compared with the best-fit templates of simulations for protons (blue), helium nuclei (green), and their sum (red). Vertical dashed lines show the cut to select proton candidates.

- Charge selection
  The PSD of DAMPE is responsible for the charge measurement of CR nuclei up to $Z = 26$. The PSD is composed of two layers placed in a hodoscopic configuration (Y-view for layer-1 and X-view for layer-2), with 41 plastic scintillator strips in each layer [14]. The deposit energy in a strip due to ionization is proportional to Z^2, which is about 2 MeV for protons. The charge is measured independently by the two PSD layers. The charge measurements of the MC simulations show an energy-dependent difference from that of the flight data primarily due to the back-scattering secondaries. To mitigate such an effect, an energy-dependent charge correction is applied for the MC data. We first parameterize the charge distributions of protons and helium nuclei in different deposited energy bins with a Landau-Gaussian convolution function for the flight data and MC data separately. Then the MC charges are shifted and shrinked according to the best-fitting parameters to match with the flight data. The combined charge distribution after corrections for low-Z nuclei for deposited energies of $447-562$ GeV is plotted in Figure 2, where the proton and helium peaks can be clearly seen. Proton candidates are selected through a cut of the PSD charge. This cut depends on the BGO deposited energy ($E_{\rm dep}$) as

$$0.6+0.05\cdot\log(E_{\rm dep}/10\ {\rm GeV}) \leq Z_{\rm PSD} \leq 1.8+0.002\cdot\log^4(E_{\rm dep}/10\ {\rm GeV}) \qquad (3.2)$$

Note that such a charge selection follows generally the logarithmic dependence of the ionization energy loss in the PSD with particle energy. The charge reconstruction efficiency is estimated independently for each PSD layer. The deviation of the flight data from the MC simulations is within 1% for layer-1 and 1.5% for layer-2.

3.2 Background

The background for protons includes mis-identified helium nuclei and a tiny fraction of electrons. Given the very good e/p separation power of DAMPE, electrons can be largely rejected [12]. The fraction of residual electrons in the proton sample is estimated to be about 0.05% for deposited energies larger than 20 GeV, using the template fit of the shower morphology parameter (ζ as defined in Ref.[13]). Helium nuclei represent the second most abundant CR component and show up as the main source of background in proton sample. To estimate the helium contamination, a template-fit method is applied to the charge distributions. The templates are obtained through MC simulations (see Figure 2). The fraction of helium contamination is $\lesssim 1\%$ for deposited energies below 10 TeV, and increases up to $\sim 5\%$ around 50 TeV.

3.3 Effective Acceptance

The effective acceptance is defined as the product of the geometric factor and selection efficiencies (including trigger, track, and charge selections). To estimate the effective acceptance, a detailed MC simulation using the GEANT4 toolkit [16] is performed. A digitization algorithm including the DAMPE detector response is developed for converting the raw energy hits by GEANT4 simulations into Analog-to-Digital Converter (ADC) counts. Then we apply the reconstruction algorithm to the simulation data to obtain the reconstructed events. An isotropic spectrum with $E^{-1.0}$ power-law is generated for detector simulation, and then is re-weighted to $E^{-2.7}$. In the analysis, the spectrum is re-weighted to $E^{-2.7}$ and then the effective acceptance of the i-th primary energy bin is obtained by

$$A_{\mathrm{eff},i} = A_{\mathrm{gen}} \times \frac{N_{\mathrm{pass},i}}{N_{\mathrm{gen},i}} \tag{3.3}$$

where A_{gen} is the geometrical factor of the MC generation sphere, $N_{\mathrm{gen},i}$ and $N_{\mathrm{pass},i}$ are the numbers of generated events and those passing the selections. The effective acceptance as a function of primary energy is shown in the *left* panel of Figure 3.

3.4 Energy Unfolding

Due to the limited thickness of the BGO calorimeter (~ 1.62 nuclear length), a proton does not fully deposit its energy in the calorimeter. The energy resolution for protons is found to be about $25\% \sim 35\%$ for incident energies from 100 GeV to 10 TeV [12]. To convert the measured energy spectrum to the primary energy spectrum, it is necessary to unfold the instrument response. Instead of correcting the particle energy event-by-event, the unfolding procedure enables an estimate of the energy distribution of incident particles from the deposit energy distribution.

The number of events in the i-th deposited energy bin, $N_{\mathrm{dep},i}$, can be obtained via the sum of number of events $N_{\mathrm{inc},j}$ in all the incident energy bins weighted by the energy response matrix

$$N_{\mathrm{dep},i} = \sum_j M_{ij} N_{\mathrm{inc},j}, \tag{3.4}$$

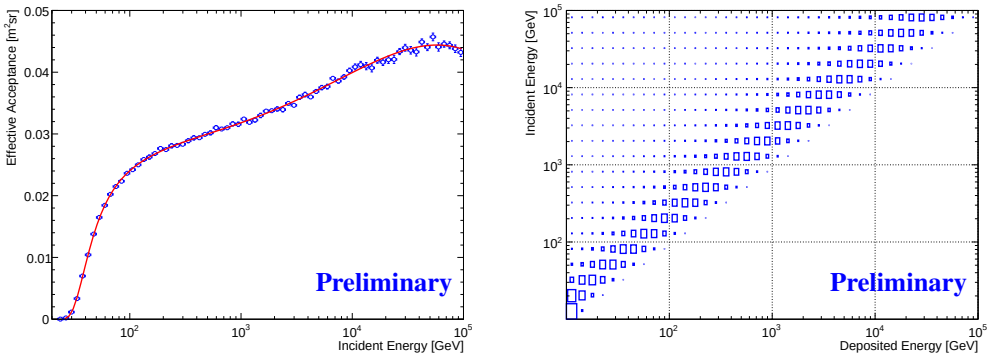

Figure 3: *Left* — The effective acceptance of proton as a function of incident energy. *Right* — Probability distribution of deposited energies in the BGO calorimeter for different incident energies, for the GEANT FTFP_BERT model.

where M_{ij}, the energy response matrix, is the probability that an event in the j-th incident energy bin is detected in the i-th deposited energy bin. The *right* panel of Figure 3 shows the energy response matrix for different incident energies, for the FTFP_BERT model [17]. Eq. 3.4 is solved with a Bayesian method to derive the incident event distribution[18].

3.5 Uncertainties

The statistical uncertainties refer to the Possion fluctuations of the detected numbers of events in each deposited energy bin. To get the statistical uncertainties of the unfolded proton fluxes, an error propagation from the detected events to the unfolded fluxes is necessary in order to properly take into account the bin-by-bin migration due to the unfolding procedure[18].

The systematic uncertainties related with the event selection are estimated through comparisons between MC simulations and the flight data. The total uncertainty of the selection efficiencies is

$$\sigma_{\rm sel} = \sqrt{\sigma^2_{\rm trigger} + \sigma^2_{\rm track} + \sigma^2_{\rm charge}} \approx 4.7\%, \tag{3.5}$$

where $\sigma_{\rm trigger} \approx 2.5\%$, $\sigma_{\rm track} \approx 3.5\%$, and $\sigma_{\rm charge} \approx 1.8\%$ are the corresponding systematic uncertainties of the trigger, track selection, and charge selection efficiencies.

The uncertainties due to the spectral deconvolution are estimated to be $\lesssim 1\%$, through regeneration of the response matrix and varying the spectral index from 2.5 to 3.1 when re-weighting the simulation data. The systematic uncertainties due to the Helium background subtraction are estimated through varying the charge selection condition Eq. 3.2 by $\pm 10\%$, and repeating the analysis. The background subtraction gives $\sim 0.1\%$ systematic uncertainties below 40 TeV and increases to $\sim 5\%$ at higher energies.

The uncertainties due to different hadronic interaction models are estimated to be about 7% for energies less than 400 GeV via comparisons of the HE trigger efficiency and the energy deposit fraction between the 400 GeV test beam data and the GEANT FTFP_BERT simulation. For higher energies, we use the difference between the GEANT FTFP_BERT model and the FLUKA model to estimate such systematic uncertainties, which vary from 7% to 10%. A further check of the

DPMJET model with the CRMC[1] interface gives negligible difference compared with the FLUKA model.

4. Results and discussion

The proton spectrum in the energy range from 40 GeV to 100 TeV is shown in Figure 4. The error bars represent the quadratic sums of statistical and systematic uncertainties. Previous measurements by space detectors PAMELA[4] and AMS-02[5], CALET [6] and balloon-borne detectors ATIC-2[3], CREAM[9], and NUCLEON[10] are overlaid for comparison. The DAMPE spectrum is consistent with those of PAMELA and AMS-02. At higher energies, our results are also consistent with that of ATIC-2, CREAM, NUCLEON and CALET when the systematic uncertainties are taken into account.

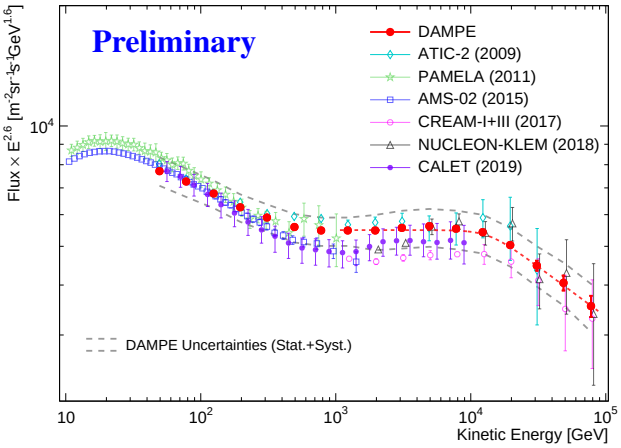

Figure 4: Proton spectrum from 40 GeV to 100 TeV measured with DAMPE (red points), compared with previous results by ATIC-2 [3], PAMELA [4], AMS-02 [5], CREAM-I+III [9], NUCLEON KLEM [10] and CALET [6]. The red error bars show the statistical uncertainties, the gray profiles show the quadratic sums of statistical and systematic uncertainties. The dashed red line indicates the best fit with a smoothly broken power law function.

The proton spectrum measured by DAMPE from 40 GeV to 100 TeV give fundamental information about the origin and propagation of Galactic CRs. A spectral hardening at a few hundred GeV energies is shown from our measurement, which is in agreement with that of previous experiments. Furthermore, the DAMPE measurement gives, for the first time, a strong evidence of a softening at about 10 TeV. We fit the spectrum for energies between 1 TeV and 100 TeV with a smoothly broken power-law model, which gives a break energy of $13.6^{+4.1}_{-4.8}$ TeV. The spectral hardening and softening are not compatible with the paradigm of a unique power-law spectrum up to the all-particle knee at PeV energies, thus implying a deep revision of CR modeling in the Galaxy.

[1] https://web.ikp.kit.edu/rulrich/crmc.html

References

[1] M. Amenomori *et al*, [The Tibet ASγ Collaboration] *The All-Particle Spectrum of Primary Cosmic Rays in the Wide Energy Range from* 10^{14} *to* 10^{17} *eV Observed with the Tibet-III Air-Shower Array*, *Astrophys. J.* **678** (2008) 1165.

[2] T. K. Gaisser, T. Stanev and S. Tilav, *Cosmic Ray Energy Spectrum from Measurements of Air Showers*, *Front. Phys.* **8** (2013) 748. [arXiv:1303.3565].

[3] A. D. Panov *et al.*, *Energy Spectra of Abundant Nuclei of Primary Cosmic Rays from the Data of ATIC-2 Experiment: Final Results*, *Bull. Russ. Acad. Sci. Phys.* **73** (2009) 564. [arXiv:1101.3246].

[4] O. Adriani *et al.* [PAMELA Collaboration], *PAMELA Measurements of Cosmic-ray Proton and Helium Spectra*, *Science* **332** (2011) 69. [arXiv:1103.4055].

[5] M. Aguilar *et al.* [AMS Collaboration], *Precision Measurement of the Proton Flux in Primary Cosmic Rays from Rigidity 1 GV to 1.8 TV with the Alpha Magnetic Spectrometer on the International Space Station*, *Phys. Rev. Lett.* **114** (2015) 171103.

[6] O. Adriani *et al.* [CALET Collaboration], *Direct Measurement of the Cosmic-Ray Proton Spectrum from 50 GeV to 10 TeV with the Calorimetric Electron Telescope on the International Space Station*. *Phys. Rev. Lett.* **122(18)** (2019) 181102.

[7] Q. Yuan, B. Zhang and X. J. Bi, *Cosmic ray spectral hardening due to dispersion in the source injection spectra*, *Phys. Rev. D* **84** (2011) 043002. [arXiv:1104.3357].

[8] N. Tomassetti, *Origin of the Cosmic-Ray Spectral Hardening*, *Astrophys. J. Lett.* **752** (2012) L13. [arXiv:1204.4492].

[9] Y. S. Yoon *et al.*, *Proton and Helium Spectra from the CREAM-III Flight*, *Astrophys. J.* **839** (2017) 1–5. [arXiv:1704.02512].

[10] E. Atkin, *et al. New Universal Cosmic-Ray Knee near a Magnetic Rigidity of 10 TV with the NUCLEON Space Observatory*. *Soviet Journal of Experimental and Theoretical Physics Letters* **108** (2018) 5.

[11] R. Alfaro, *et al.* [HAWC Collaboration], *All-particle cosmic ray energy spectrum measured by the HAWC experiment from 10 to 500 TeV*. *Phys. Rev. D*, **96** (2017) 122001. [arXiv:1710.00890].

[12] J. Chang *et al.* [DAMPE Collaboration], *The Dark Matter Particle Explorer mission*, *Astropart. Phys.* **95** (2017) 6–24. [arXiv:1706.08453].

[13] G. Ambrosi, *et al.* [DAMPE Collaboration], *Direct detection of a break in the teraelectronvolt cosmic-ray spectrum of electrons and positrons*. *Nature* **552** (2017) 63–66.

[14] Y. H. Yu *et al.*, *The Plastic Scintillator Detector at DAMPE*, *Astropart. Phys.* **94** (2017) 1–10. arXiv:1703.00098

[15] E. ThÃl'bault *et al.*, *International Geomagnetic Reference Field: the 12th generation*, *Earth, Planets and Space* **67** (2017) 79.

[16] S. Agostinelli, *et al.*, *Geant4 - a simulation toolkit Nucl. Instrum. Meth. A* **506** (2017) 3.

[17] Geant4 version employs FTFP_BERT as a recommended physics list for the simulation of high energy hadronic showers. *http://geant4-userdoc.web.cern.ch/geant4-userdoc/UsersGuides/PhysicsListGuide/html/physicslistguide.html*

[18] G. D'Agostini. *A multidimensional unfolding method based on Bayes' theorem*, *Nuclear Instruments and Methods in Physics Research A* **362** (1995) 362.